



## Pillared HMCM-36 zeolite catalyst for biodiesel production by esterification of palmitic acid

Ralitsa Purova<sup>b</sup>, Katabathini Narasimharao<sup>a,\*</sup>, Nesreen S.I. Ahmed<sup>a</sup>, Shaeel Al-Thabaiti<sup>a</sup>, Abdulmohsen Al-Shehri<sup>a</sup>, Mohammed Mokhtar<sup>a,\*</sup>, Wilhelm Schwieger<sup>b</sup>

<sup>a</sup> Department of Chemistry, Faculty of Science, King Abdulaziz University, P.O. Box 80203, Jeddah 21589, Saudi Arabia

<sup>b</sup> Institute of Chemical Reaction Technology, University of Erlangen-Nuremberg, Germany

### ARTICLE INFO

#### Article history:

Received 19 March 2015

Received in revised form 3 June 2015

Accepted 4 June 2015

Available online 6 June 2015

#### Keywords:

Pillared HMCM-36

MCM-22(P)

Biodiesel

Esterification

Palmitic acid

### ABSTRACT

Layered MWW zeolite has been studied for swelling/pillaring using CTAB and silica as swelling and pillaring reagents, respectively to synthesize pillared MCM-36 material. The swelling/pillaring efficiency was evaluated based on their X-ray diffraction, N<sub>2</sub>-physisorption, scanning electron microscopy and FTIR spectra after pyridine adsorption as indicator for acidity measurements and catalytic potential. There was an overall decrease in acid site concentration due to incorporation of inert silica pillars. However, after ion exchange, mesoporous HMCM-36 zeolite with the highest BET surface area showed increased Brønsted and Lewis acid sites compared to the MCM-22, suggesting enhanced accessibility of acid sites for bulky reacting molecules. MCM-22 and MCM-36, as well as the ion exchanged HMCM-22 and HMCM-36 samples were tested for esterification of palmitic acid with methanol. The HMCM-36 catalyst showed high activity in palmitic acid esterification with methanol. This catalyst can be readily separated from the reaction system for re-use for at least four cycles without losing any activity suggesting potential industrial applications in biodiesel synthesis.

© 2015 Elsevier B.V. All rights reserved.

### 1. Introduction

Zeolites are solid catalysts which are used commercially in many industrial processes [1]. Zeolites can be used as shape-selective catalysts due to their well-defined pores with minimum kinetic diameters similar to the size of small organic molecules [2]. However, for some chemical processes, these catalysts are required to catalyze reactions involving larger, bulkier molecules. Researchers studied two classes of materials to fulfill this requirement: (i) mesoporous M41S-type materials and (ii) pillared or delaminated layered materials. The M41S family has been extensively investigated regarding the formation, characterization of their porous structure and catalytic applications [3]. However, these materials possess significantly weaker acid sites than the acid sites presented in micro porous zeolites [4]. Thus, materials with acid sites of strength similar to those in zeolites, which are accessible to large organic molecules, are of general interest. We recently synthesized

partially crystalline nanosized ZSM-5 zeolites with high surface area and meso–macro pore volume [5]

Pillared layered structures are built of inorganic layers with inorganic or organic pillars appended on both sides of the sheets [6]. These materials are potentially most attractive for catalysis, because they combine high specific surface areas and good accessibility for larger molecules to a large number of catalytic sites [7]. MCM-22 zeolite with its MWW structure and acidic properties holds interesting opportunities for different structure modifications and catalytic applications [8].

Currently, there is an enormous interest in the catalytic esterification reaction because of its application in several industrial processes [9]. One of the main products obtained by esterification of long chain fatty acids is biodiesel, an attractive bio-renewable fuel which has environmental benefits over conventional petroleum based fuels [10]. For an alkali catalyzed transesterification, the glycerides and alcohol must be free from water and FFAs since the presence of free fatty acids (FFAs) causes deactivation of homogeneous alkali catalysts such as NaOH and KOH by forming soaps and creating difficulties to separate the products [11]. Taking into account that some of the natural vegetable oils or animal fats contain considerable amounts of FFAs, which interfere with the transesterification process and must be converted into their corre-

\* Corresponding authors. Fax: +966 26952292.

E-mail addresses: [katabathini@yahoo.com](mailto:katabathini@yahoo.com), [nkatabathini@kau.edu.sa](mailto:nkatabathini@kau.edu.sa) (K. Narasimharao), [mmokhtar2000@yahoo.com](mailto:mmokhtar2000@yahoo.com) (M. Mokhtar).

sponding esters before reaction, pre-esterification appears as an essential step in the production of biodiesel from acid oils [12].

Esterification is normally carried out in the homogeneous phase in the presence of acid catalysts such as sulfuric and *p*-toluene sulfonic acids. This pretreatment step has been successfully demonstrated using sulfuric acid [13]. Unfortunately, use of the homogeneous sulfuric acid catalyst adds neutralization and separation steps as well as the esterification reaction to the process and also has several drawbacks such as equipment corrosion, difficulty of handling, and problems separating the products from the catalysts [11]. The use of heterogeneous catalysts can be an alternative to reduce biodiesel cost. Various heterogeneous catalysts such as zeolites (HUSY, HBEA, HMOR, HZSM-5 and HMCM-22), sulfated oxides ( $\text{SnO}_2$ ,  $\text{ZrO}_2$ ,  $\text{Nb}_2\text{O}_5$  and  $\text{TiO}_2$ ), heteropolyacids (12-tungstophosphoric acid) and commercial sulfonic resin (Amberlyst-15) were used for esterification of FFAs [14]. However, catalysts with micropores are not suitable for biodiesel production because the micropores limit the diffusion of large molecules with long alkyl chains [15]. Conceptually, the high acid strength and uniform mesopores offer an unprecedented tool to control catalytic conversion in acid catalyzed reactions [16].

The catalytic activity of MCM-22 and pillared MCM-36 material has not been systematically explored for fatty acid esterification, hence the present work seeks to improve our fundamental understanding of structure, texture and acidity relations and the concomitant catalytic activity of MCM-22 and pillared MCM-36 solid acids in the low temperature esterification of palmitic acid with methanol for application in biodiesel production.

## 2. Experimental

### 2.1. Synthesis of materials

#### 2.1.1. MCM-22(P)

Layered precursor, MCM-22(P) was hydrothermally synthesized using hexamethylenimine (HMI, 99% Aldrich), Aerosil 200 (Degussa), sodium aluminate (53%  $\text{Al}_2\text{O}_3$ , 43%  $\text{Na}_2\text{O}$ , Riedel de Haen), sodium hydroxide (25% solution prepared from pure pellets, Merck) and deionized water. In a typical synthesis method, solution 'A' was prepared by dissolving  $\text{NaAlO}_2$  (1.8 g) in water (200.2 g) and solution 'B' by mixing 25% NaOH solution (20.1 g) and water (348.1 g) and stirred for 10 min. Then both A and B were mixed, HMI (41.0 g) added to the solution and stirred for 45 min. After that the solution was put in water bath at 50 °C and Aerosil (49.87 g) was added on portions under vigorous stirring. Finally 40 g of  $\text{H}_2\text{O}$  was added to the synthesis mixture and stirred for 2 h. The chemical composition of the final gel was: 1  $\text{SiO}_2$ : 0.09  $\text{Na}_2\text{O}$ : 0.5 HMI: 45  $\text{H}_2\text{O}$ : 0.01  $\text{Al}_2\text{O}_3$ . The synthesis was carried out in 1 L autoclave, stirring speed 600 rpm, crystallization temperature and time were 135 °C and 8 days, respectively. The crystalline product was collected by centrifugation at 10,000 rpm, washing with distilled water and subsequently dried at 75 °C overnight.

#### 2.1.2. Calcination of MCM-22(P) to MCM-22

MCM-22 sample was obtained by calcination of MCM-22(P) at 550 °C (1 °C  $\text{min}^{-1}$  rate) for 5 h under the flow of air.

#### 2.1.3. Swelling and pillaring of MCM-22(P) to synthesize MCM-36

MCM-22(P) was swollen following the procedure reported by Corma et al. and Maheshwari et al. [8]. The layered precursor was mixed with hexadecyltrimethylammonium bromide (CTAB, 98% Sigma-Aldrich), tetrapropylammonium hydroxide (TPAOH, 40% Süd Chemie) and water in a weight ratio of 1.8 g MCM-22(P): 10.1 g CTAB: 4.4 g TPAOH: 38.6 g  $\text{H}_2\text{O}$ . The mixture was allowed to stir for 48 h at 40 °C after that the particles were recovered by repeated cycles of centrifugation, washing with distilled water and drying

at 75 °C overnight. Pillaring was carried out with 1 g of solid dried swollen material and 6 g of tetraethyl orthosilicate (TEOS, 98% Alfa Aesar). The mixture was then placed in an oil bath at 80 °C and stirred for 24 h. After what the samples were removed and filtered using Whatmann's filter paper and dried in an oven at 30 °C for 12 h to remove the TEOS excess. Dried samples were then mixed with water in a 1:10 weight ratio to undergo hydrolysis for 5 h at 40 °C, after that they were filtered by gravity and dried at 30 °C. Pillared samples were calcined in a muffle oven using two steps calcination procedure. In the first step heating rate was set at 1 °C per min to 450 °C under nitrogen stream and this temperature was maintained for 6 h. Finally the samples were kept at 550 °C under air for 12 h (temperature ramp rate of 2 °C per min).

#### 2.1.4. Ion exchange

MCM-22 and MCM-36 after calcination were ion-exchanged with an excess of 1  $\text{mol L}^{-1}$   $\text{NH}_4\text{NO}_3$  aqueous solution (liquid-to-solid ratio of 10  $\text{cm}^3 \text{g}^{-1}$ ) and stirred continuously at room temperature for 8 h. The pH of the mixture was adjusted to 7 with  $\text{NH}_4\text{OH}$ . This procedure was repeated twice. After filtering and drying, the resulting  $\text{NH}_4^+$  forms of MCM-22 and MCM-36 were calcined at 500 °C for 5 h in air to obtain HMCM-22 and HMCM-36 samples.

### 2.2. Characterization of materials

The elemental composition of the catalysts was determined by ICP-MS, Optima 7300DV, PerkinElmer Corporation, USA. The sample preparation for ICP-MS is as follows; about 100 mg of catalyst was placed in a PTFE beaker and then complete dissolution of the sample was achieved by adding 8 mL of 40% HF, 2 mL of  $\text{HNO}_3$  and 2 mL HCl and to this 15 mL of ultra-pure water was added and then PTFE beaker was placed in ultrasonic bath for 10 min to obtain homogeneous dissolution. The solution was then rinsed into a centrifuge tube and centrifuged at 3000 rpm for 3 min. The clear supernatant was decanted and used to prepare 250 mL stock solution.

XRD diffraction patterns were obtained from X'pert Pro diffractometer from Phillips Analytical.  $\text{CuK}\alpha$  radiation ( $\lambda = 1.54056 \text{ \AA}$ ) was used. The samples were measured in sample holders with a smaller exposure area. Diffraction patterns of the samples after synthesis, swelling and calcination were measured by using the following program:  $2\theta$  angle from 2 to 30° with a step of 0.02° and increasing duration of 5 s per step.

Morphology of the samples (scanning electron microscopy images) was determined by using Carl Zeiss ULTRA55 microscope equipment at a 3 kV voltage and magnifications at magnitude 10,000.

Nitrogen-sorption measurements were performed by first carrying out a pre-treatment of the samples. During pre-treatment the samples were heated with a 1 °C per min rate to 250 °C under high vacuum, and kept at these conditions for 12 h. Analysis measurements were performed using Micromeritics ASAP 2010 instrument at a temperature of –196 °C.

DRIFT spectra of calcined catalysts obtained at room temperature using Perkin-Elmer Spectrum 100 FTIR spectrometer. Then, the samples were subjected to a pyridine adsorption analysis. The analysis was carried out over a catalyst disk which was treated at 100 °C under vacuum for 5 h. Later, the sample was treated with pyridine vapor and finally heated at 100 °C under vacuum for 30 min. DRIFT spectra were collected at room temperature. The amount of Brønsted and Lewis acid sites was calculated via integration of the area of the absorption bands showing the maximum values of intensity at 1446 and 1536  $\text{cm}^{-1}$ , respectively. Integrated absorbance of each band was obtained using the appropriate software by applying the

corresponding extinction coefficient and normalized by the weight of the samples.

Ammonia temperature programmed desorption (TPD) measurements were performed to titrate the total number of acid sites, using CHEMBET-3000 (Quantachrome, USA) equipped with TCD detector, PID-controlled furnace heated flow microreactor. Calculated amount of catalyst sample (250 mg) was pretreated at 120 °C for 2 h under helium gas flow (80 mL min<sup>-1</sup>). The gas flow was switched to ammonia to saturate the sample for 1 h and then the sample flushed by helium gas at 100 °C for 2 h to remove physisorbed ammonia prior to recording the TCD signal. The desorption patterns were recorded by ramping the temperature of the sample to 800 °C at a rate of 10 °C min<sup>-1</sup> under a steady flow of helium gas (80 mL min<sup>-1</sup>). The amount of ammonia evolved was determined by comparing the areas desorbed from the sample with those of known amounts of injected ammonia.

### 2.3. Esterification of palmitic acid

Esterification reactions were performed in a stirred batch reactor with samples withdrawn periodically for analysis using a Shimadzu GC17A Gas Chromatograph fitted with a DB1 capillary column (film thickness 0.25 mm, id 0.32 mm, length 30 m). Reactions were performed at 70 °C using 0.05 g of catalyst, 5 mmol of palmitic acid, 0.0025 mol (0.587 mL) hexyl ether as internal standard, and 0.3036 mol (12.5 mL) methanol. Reaction profiles were followed for a period of 6 h and continued for 24 h to assess limiting conversions.

## 3. Results and discussion

Lamellar MWW zeolite precursor such as MCM-22(P) offers unprecedented opportunities for creating diversity of more open zeolite structures by expanding and modifying the interlamellar space (as shown in Scheme 1) [17]. The swelling and pillaring procedures are easy, least destructive and most efficient expansion of layered zeolites. In this study, CTAB solution with high pH was used to provide swollen MCM-22 that can be converted to the pillared MCM-36 with large pores. High pH of the swelling solution was obtained by addition of tetrapropylammonium hydroxide to the CTAB solution.

ICP-MS analysis was used to determine the chemical composition of the synthesized precursor. The analysis revealed that Si/Al ratio of the MCM-22(P) sample is 34.4, which was less than the starting composition of the synthesis substrate mixture of Si/Al = 50. Thus, these results suggest that the incorporation of silicon was smaller than that expected considering its amount present in the synthesis gel.

Fig. 1 shows the powder XRD patterns of MCM-22 and MCM-36 samples before and after the ion exchange. The as-synthesized MCM-22 is a two-dimensional layer with a hexagonal pore structure (Scheme 1). The XRD patterns of MCM-22 samples show a small characteristic reflection (002) at 6.58°, which corresponds to the unit cell parameter 'c'. This peak disappears in the XRD pattern for swollen and pillared MCM-36 samples. In addition, the pillared MCM-36 samples show (001) peak around 2θ = 2° corresponding to an interlayer distance of about 4.5 nm, which indicates successful pillaring [7]. The two diffraction peaks corresponding to (101) and (102) reflections appeared distinctively in MCM-22 samples, in contrast a broad band can be observed in this region for the MCM-36 samples, which is an indication of loss of registry along the c-axis due to the introduction of pillars [19]. The XRD patterns of MCM-22 and MCM-36 samples are in good agreement with those previously published report [20].

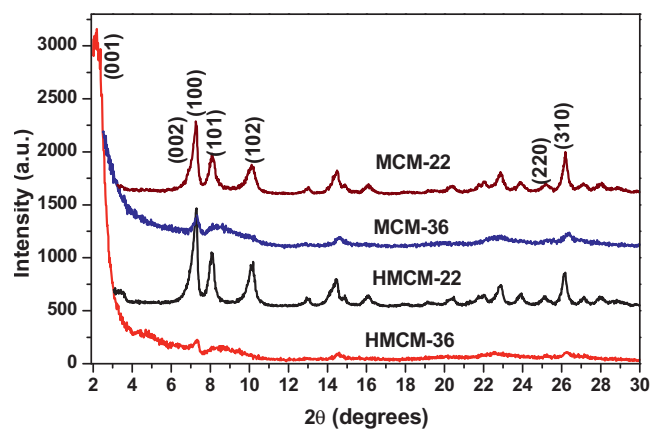


Fig. 1. XRD patterns of the samples.

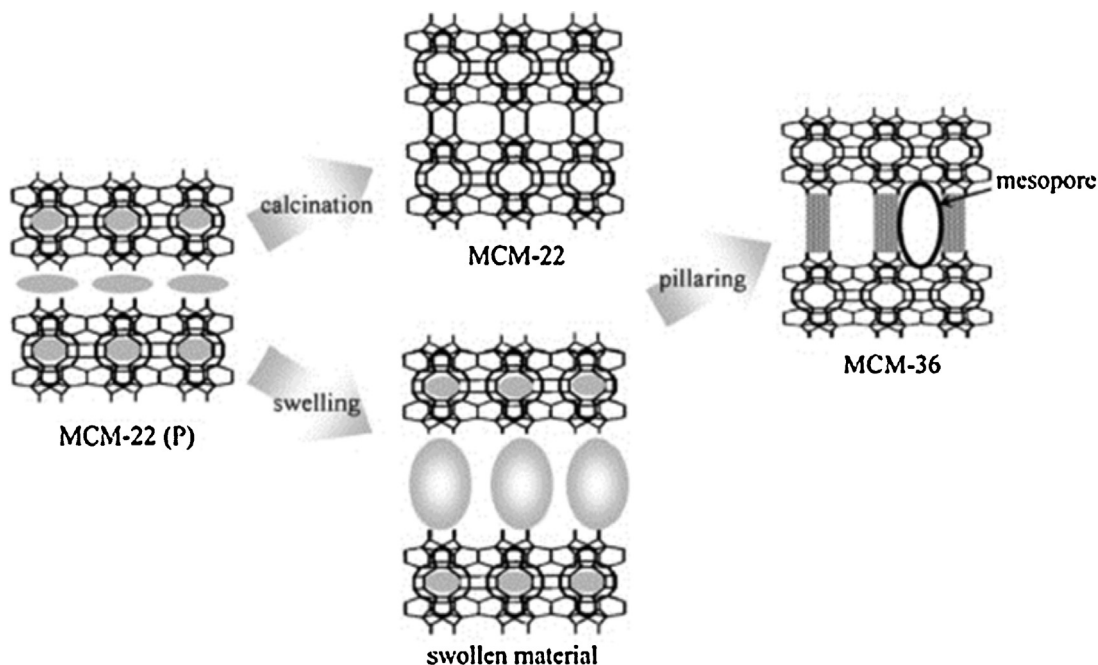
Table 1

Surface area and pore volume of the samples from N<sub>2</sub>-adsorption measurements.

Sample	Surface area (m <sup>2</sup> g <sup>-1</sup> )			Pore volume (cm <sup>3</sup> g <sup>-1</sup> )		
	S <sub>BET</sub>	S <sub>micro</sub>	S <sub>meso</sub>	V <sub>total</sub>	V <sub>micro</sub>	V <sub>meso</sub>
MCM-22	492	399	93	0.52	0.16	0.36
HMCM-22	449	332	117	0.58	0.11	0.47
MCM-36	907	385	522	0.97	0.19	0.78
HMCM-36	635	205	430	0.85	0.04	0.81

Scanning electron microscopy (SEM) was employed for the direct visualization of crystal morphology and layer structure of the samples. SEM images of MCM-22 and MCM-36 samples before and after ion exchange are shown in Fig. 2. Morphology of MCM-22 samples indicating that the material consists of thin irregular platelets that are about 500–1000 nm in diameter and 50–100 nm in thickness. MCM-36 samples shows preservation of crystal morphology after the swelling and pillaring process. The crystals retain their platelets morphology and sharp facets as seen in Fig. 2 (the crystals are oriented along their thinner edge in this image). Pillared MCM-36 samples had more highly agglomerated parts than MCM-22 samples; this is probably due to condensation of surface Si–OH groups after thermal treatment. The SEM images of the MCM-22 samples clearly showed platelet morphology. In contrast, MCM-36 samples shows some large particles are formed by the aggregation of these platelets with distinctive platelet structure. He et al. [7] attributed this change of morphology to the silica pillars between layers of swollen MCM-22 resulting in increase of the platelet thickness. The XRD patterns are clearly indicating that the loss of crystallinity in case of MCM-36 samples compared to MCM-22 samples. This is due to fact that these samples possessed more silica than the MCM-22 samples. The observations from the XRD measurements agree well with the changes in morphology revealed by SEM analysis.

Nitrogen adsorption-desorption isotherms and BJH pore size distributions of the samples are shown in Fig. 3(A) and (B), respectively. The MCM-22 sample showed a type I isotherm in accordance with the microporous nature of the material, on the other hand, pillared MCM-36 showed type IV isotherm with a hysteresis loop at P/P<sup>o</sup> = 0.4 for capillary condensation. This observation suggests that the swelling and subsequent pillaring led to the formation of mesopores. The textural properties of the two samples are presented in Table 1. The BET surface area (S<sub>BET</sub>) of pillared MCM-36 was substantially higher than that of MCM-22. The micropore volume (0.16 cm<sup>3</sup> g<sup>-1</sup>) for MCM-22 sample corresponds only to 30% of the total pore volume (0.52 cm<sup>3</sup> g<sup>-1</sup>) and also the hysteresis loop of this sample can be observed at p/p<sup>o</sup> > 0.90 with asymptotic growth to p/p<sup>o</sup> → 1. This hysteresis loop can be indicative of the filling of



**Scheme 1.** Schematic representation of MCM-22(P) and its derivatives [18].

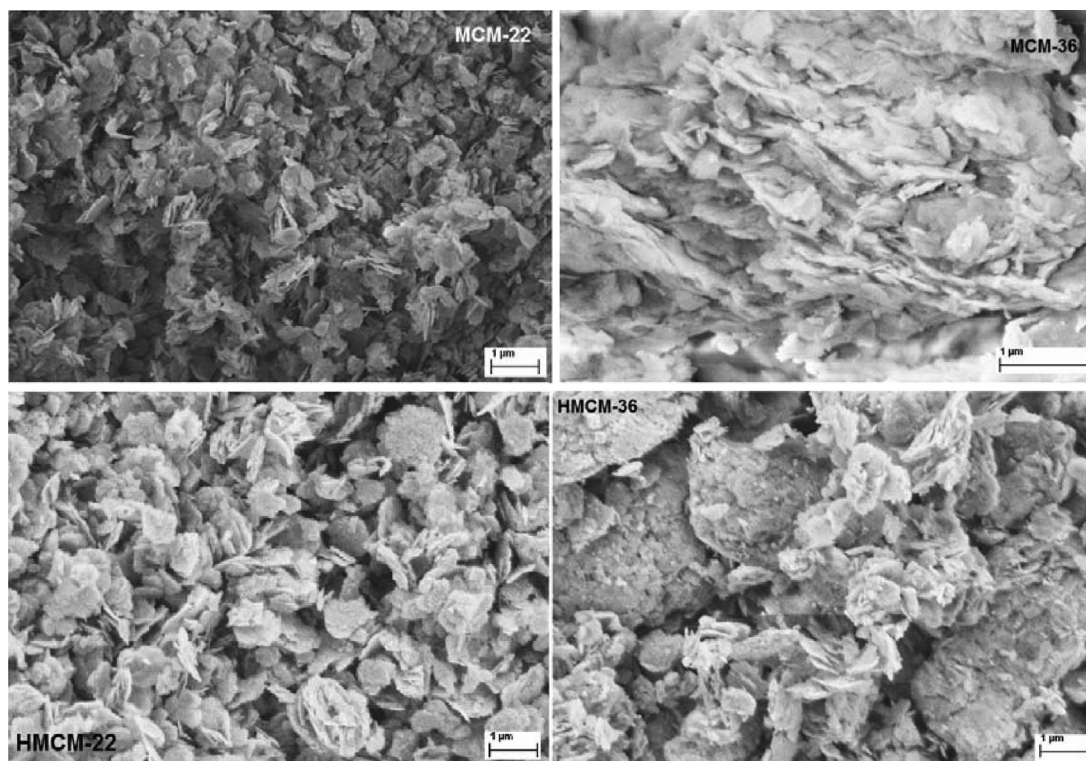


**Fig. 2.** SEM images of the samples.

the space among the particles with the adsorbate ( $N_2$  gas) and not to the filling of mesopores. On the other hand, the MCM-36 sample showed total pore volume ( $0.97 \text{ cm}^3 \text{ g}^{-1}$ ) with mesopores of  $0.78 \text{ cm}^3 \text{ g}^{-1}$ . The changes of micropore volume,  $V_{\text{micro}}$  and mesopore volume,  $V_{\text{meso}}$  reflect structural changes caused by the swelling followed by pillaring.

A small decrease in the surface area (from  $492$  to  $449 \text{ m}^2 \text{ g}^{-1}$  in case of MCM-22) was observed after ion exchange. The difference is high in case of pillared MCM-36 sample. A similar observation was

reported by Lasperas et al. [21]. The authors suggested that the loss of surface area was caused by breakage of Si–O–Si bonds leading to pore collapse.

The BJH pore size distribution for the two samples is shown in Fig. 3(B). The results presented in Fig. 3(B) clearly indicating that the MCM-36 samples has mesopores, on other hand major porosity exists in the micropore region for the MCM-22 samples. The mesoporous distribution formed with a cylindrical or slit-shaped pore model shows an intense maximum at  $2.5$ – $3.0 \text{ nm}$  in MCM-36

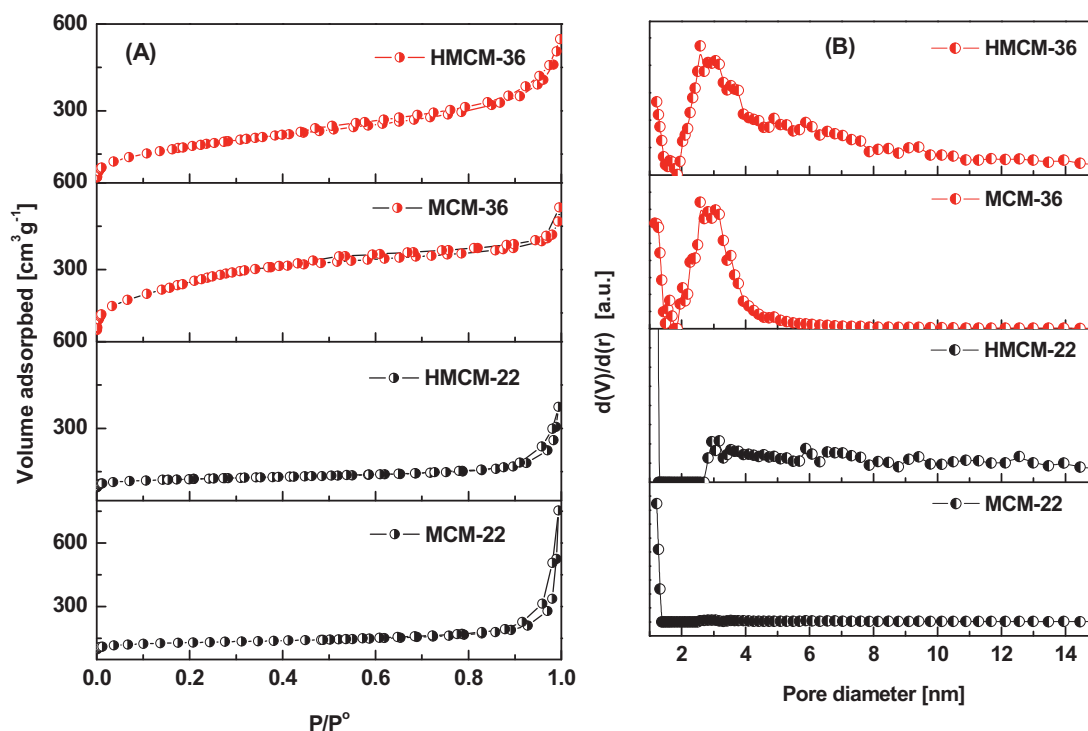


Fig. 3. (A)  $N_2$  adsorption-desorption isotherms and (B) BJH pore size distribution of the samples.

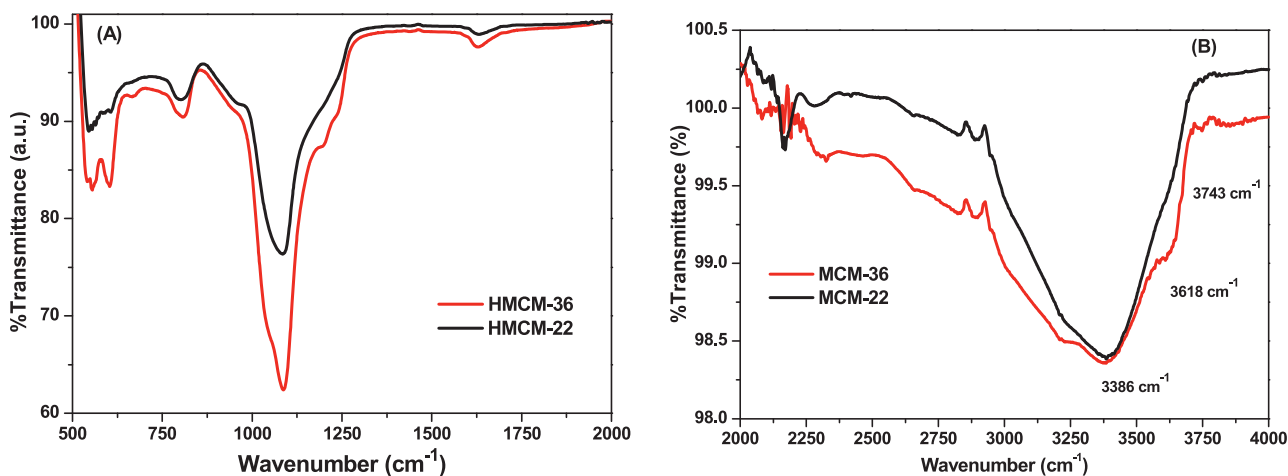


Fig. 4. FTIR spectra of the samples in the region of (A) 500–2000  $cm^{-1}$  (B) 2000–4000  $cm^{-1}$ .

and these mesopores are formed in this sample due to swelling-pillaring and calcination procedures.

The FTIR spectrum of MCM-22 precursor and pillared MCM-36 samples in the range of 500–2000  $cm^{-1}$  are shown in Fig. 4(A). The bands at 1087  $cm^{-1}$  and 1035  $cm^{-1}$  correspond to internal asymmetric stretching, and the bands at 595  $cm^{-1}$  and 554  $cm^{-1}$  are attributed to the presence of double rings in the MCM-22 structure. The band at 805  $cm^{-1}$  corresponding to external symmetrical stretching vibration was observed in both the samples. Another small band at 1630  $cm^{-1}$  which can be ascribed to the angular deformation of the O–H bond [22] was also observed in both samples.

The presence of bands related to the symmetrical and asymmetrical stretching of the O–H groups present in the MCM-22 and MCM-36 samples was also investigated (Fig 4(B)). A broad band around 3386  $cm^{-1}$  appeared for both samples and can be

attributed to the adsorbed asymmetric stretching vibration of water molecules and surface hydroxyl groups. A small band at 3743  $cm^{-1}$  due to Si–OH was appeared for pillared MCM-36 sample, which is indicative of Si–OH groups located on the outer termination of  $SiO_2$  pillars present between the zeolite layers in this sample. It is interesting to note that this band was not clearly appeared in case of MCM-22 sample, this is probably due to very low concentration of isolated Si–OH species on the external surface of this sample [23]. A band at 3618  $cm^{-1}$ , which can be assigned to strong Brönsted acidic bridging hydroxyl groups (Si–OH–Al) [24] can be observed in both the samples, however the intensity of this peak is relatively higher in MCM-36 sample than MCM-22.

The major goal of this work is to synthesize pillared MCM-36 material to generate a better catalyst in comparison to the untreated zeolite.

**Table 2**  
Data from DRIFT pyridine adsorption measurements of samples.

Sample	Number of acid sites ( $\mu\text{mol g}^{-1}$ )		B/L ratio	Number of total sites ( $\mu\text{mol g}^{-1}$ )
	Brønsted (B)	Lewis (L)		
MCM-22	0.0	13.6	–	13.6
HMCM-22	4.2	15.8	0.265	20.0
MCM-36	0.0	10.8	–	10.8
HMCM-36	34.3	10.2	3.362	44.5

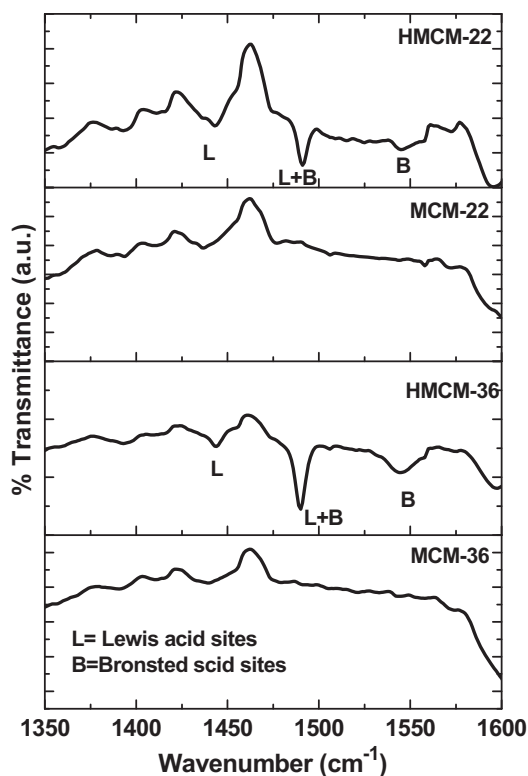


**Fig. 5.** FTIR spectra of the MCM-22, HMCM-22, MCM-36 and HMCM-36 samples after the pyridine adsorption.

It is known that the presence of inert pillars in MCM-36 puts the pillared derivative at a disadvantage by diminishing overall acidity, while the process of swelling and pillaring may degrade the existing centers [25]. To avoid this disadvantage, we performed the ion exchange of sodium ions with protons, which could increase the overall acidity of the pillared MCM-36 material. The acidic properties of as synthesized and ion exchanged samples were evaluated using FTIR spectroscopy following pyridine adsorption. The results are shown in Fig. 5 and Table 2. As-synthesized samples showed only peak corresponding to Lewis acid sites. In contrast, the ion exchanged samples showed peaks due to Brønsted and Lewis acid sites. In comparison, the ion exchanged MCM-22 sample showed lesser number of Brønsted acid sites and almost same amount of Lewis acid sites as pillared HMCM-36 sample. The spectra of these two samples displayed well resolved bands at 1443, 1490 and 1545  $\text{cm}^{-1}$ . The band at 1443  $\text{cm}^{-1}$  can be assigned to characteristic of Lewis-coordinated pyridine (L), whereas the band at 1545  $\text{cm}^{-1}$  was due to Brønsted coordinated pyridine (B), and the band at 1490  $\text{cm}^{-1}$  is due to Lewis and Brønsted -coordinated pyridine (L + B). The assignment of these bands was in agreement with those reported in the literature [26].

The HMCM-22 sample predominantly exhibited Lewis acidity with a minor contribution of Brønsted acidity. However, major differences were noticed in FTIR spectrum of HMCM-36 sample. The

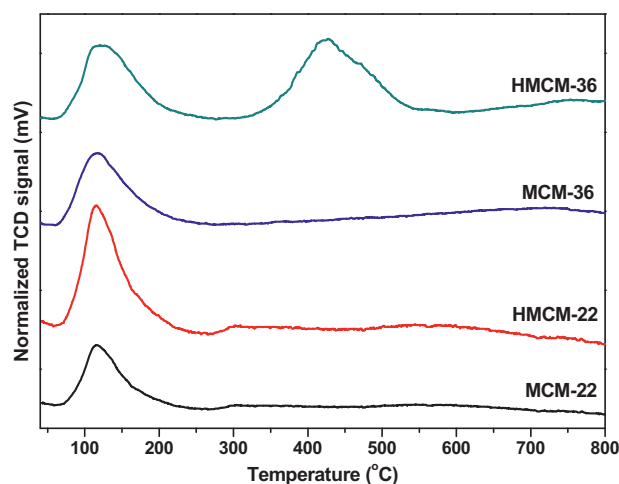


**Fig. 6.**  $\text{NH}_3$ -temperature programmed desorption profiles of the samples.

formation of new Brønsted sites was clearly observed as revealed by the intense band at 1545  $\text{cm}^{-1}$  along side of intense peak due to Lewis and Brønsted acid sites. The concentration of the Brønsted acid (B) sites and Lewis acid (L) sites were determined based on intensities of the bands observed at 1545 and 1443  $\text{cm}^{-1}$ , taking the corresponding molar extinction coefficients ( $\epsilon$ ), i.e.,  $0.059 \pm 0.004$  and  $0.084 \pm 0.003 \text{ cm}^2 \text{ mol}^{-1}$ , respectively [27]. Quantitative data were calculated using the Lambert–Beer equation [28] listed in Table 2. It is clearly shown from Table 2 that ion exchange resulted increase of the Brønsted acid sites concentration. It is known that Si/Al ratio plays an important role in the final concentration of acidic sites in zeolites.

The concentration and distribution of acid sites in MCM-22 and pillared MCM-36 samples before and after ion exchange were characterized by temperature programmed desorption (TPD) of ammonia (Fig. 6). The TPD profiles of the MCM-22 samples showed a maximum desorption peak at 115 °C and a small peak at 335 °C. Unverricht et al. [29] and He et al. [7] attributed the low temperature peak to the physisorbed ammonia desorbed from the samples, whereas the small peak at approximately 335 °C is assigned to the desorption of  $\text{NH}_4^+$  ions from strong Brønsted acid sites. A broad peak is observed in the range between 350 and 575 °C, with maximum near 450 °C in the pattern of HMCM-36 sample, which could be ascribed to strong Brønsted acid sites generated during the swelling and calcination procedure.

It can be easily seen that at a given Si/Al ratio in the final pillared material, the swelling procedure gives a sample with much higher concentration of Brønsted acid sites and with a higher proportion of sites with medium-to-strong acidity. This result is important from the catalytic point of view, since activity and selectivity of the catalyst will be related to the total number of Brønsted acid sites and their acid strength distribution. The acid site concentration of pillared MCM-36 is significantly higher compared to MCM-22. These results are in quite accordance with the FTIR analysis after pyridine adsorption.

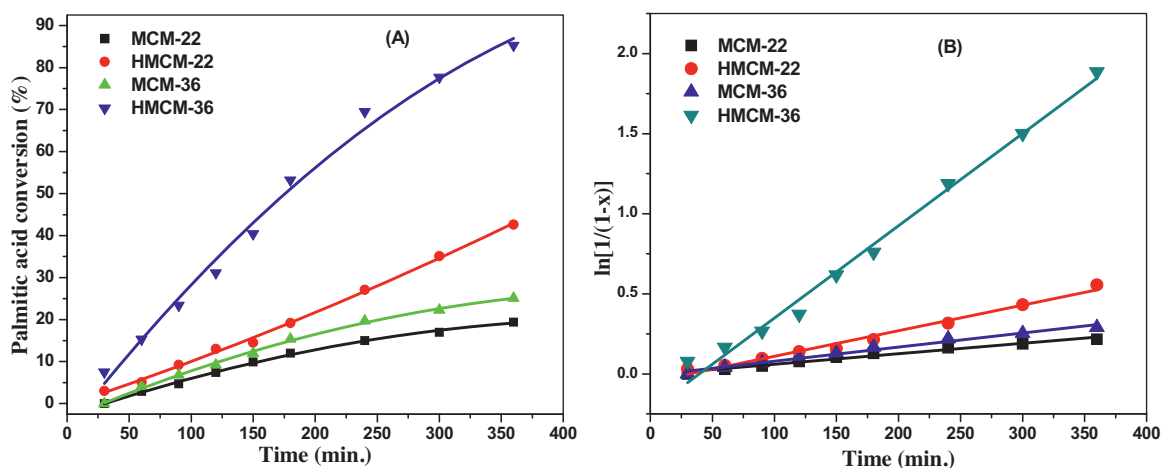


Fig. 7. (A) Effect of reaction time on the conversion of palmitic acid over all the samples (B) A plot between  $[\ln 1/(1-x)]$  and reaction time (reaction temperature; 70 °C).

Table 3

Comparison of the kinetic performance of the functionalized mesoporous silica catalysts.

Catalyst	Apparent activation energy (kJ mol <sup>-1</sup> )	Rate constant (min <sup>-1</sup> ) × 10 <sup>-4</sup>			Conversion of palmitic acid (%) <sup>a</sup>
		70 °C	80 °C	90 °C	
MCM-22	58.86	6.6	8.9	9.5	26
HMCM-22	48.09	16.0	35.9	45.9	60
MCM-36	62.12	8.8	12.0	20.3	39
HMCM-36	21.58	57.6	119.5	171.5	100

<sup>a</sup> Conversion of palmitic acid after 24 h reaction, reaction temperature; 70 °C.

Table 4

Comparison of activity of different mesoporous catalysts in esterification of palmitic acid with methanol.

Mesoporous catalyst	Reaction conditions	Conversion of Palmitic acid (%)	Reference
HPA/SBA-15	30 mL of MeOH, 8 mmol of PA, temperature = 60 °C; catalyst wt.; 0.2 g. reaction time; 6 h	90	[14]
WO <sub>x</sub> /ZrP	60 °C, 30:1 molar ratio MeOH:PA; reaction time; 6 h	78	[12]
WO <sub>x</sub> /ZrO <sub>2</sub>	60 °C, 30:1 molar ratio MeOH:PA; reaction time; 6 h	30	[33]
Al-MCM-41	0.6 wt% catalyst at a 60/1 alcohol/PA ratio, 130 °C for 2 h	79	[34]
SO <sub>3</sub> H-SWCNHs	Catalyst wt., PA and MeOH = 0.15, 0.15, and 5 g; temperature = 64 °C; reaction time; 5 h	90	[35]
SBA-15-SO <sub>3</sub> H-P123	1:20 w/w (PA:MeOH) in oil, 85 °C, 3 h	95	[11]
Pillared HMCM-36	80 °C, 12.5 mL MeOH, 30:1 molar ratio MeOH:PA acid; reaction time; 6 h	100	Present work

The catalytic activity of the as-synthesized and ion exchanged MCM-22 and pillared MCM-36 samples for the esterification of palmitic acid with methanol was determined. Fig. 7(A) shows the effect of reaction time on the conversion of palmitic acid over all the samples. We determined the degree of conversion as a function of time under the identical reaction conditions (reaction temperature 70 °C, alcohol/acid molar ratio of 60, 0.05 g catalyst). It was observed that the catalytic activity decreases in the series: HMCM-36 > HMCM-22 > MCM-36 > MCM-22. This behavior can be explained due to the HMCM-36 catalyst possessing the highest acid strength of studied catalysts (Table 2). After 6 h of reaction, it was observed that the palmitic acid conversion (%) is 85.3%, 42.6%, 25.1 and 19.4% for the HMCM-36, HMCM-22, MCM-36 and MCM-22 catalysts, respectively. The values of the maximum conversion obtained by the solid HMCM-36, HMCM-22, MCM-36 and MCM-22 catalysts within 24 h are shown in Table 3. It can be clearly seen that HMCM-36 has the highest catalytic performance.

The order of the esterification reaction was determined by following the classical definitions of chemical kinetics. Considering the conditions employed in the process, palmitic acid is a limiting reagent. Fig. 7(B) shows possible fits of the esterification reaction of palmitic acid assuming first-order kinetics. The fitting in Fig. 7(B) reveals a linear relation between all experimental data when  $[\ln 1/(1-x)]$  is plotted as a function of reaction time, thus establish-

ing the existence of a first-order dependence between the reaction rate and the concentration of palmitic acid for the esterification reaction. The regression coefficients of the straight lines show good fits to first-order kinetics. Several reports in the literature establish first-order kinetics for this esterification reaction [30].

It was reported that higher number of acid sites and larger pore diameter of catalyst could contribute to the improved performance in esterification of palmitic acid. The responsible factor of the high activity for the HMCM-36 catalyst requires understanding of the relative importance of its superiority in pore size and number of acid sites. To understand these features, the esterification was performed for all the catalysts at a range of temperatures from 70 to 90 °C (Fig. 8). The collected data was used to calculate apparent activation energies for the catalysts.

The apparent activation energies were calculated assuming a pseudo-first-order reaction with respect to the palmitic acid. The calculated rate constants and apparent activation energies are summarized in Table 3 for all the catalysts. A temperature increase of 10–20 °C caused an increase in the rate constants. The ion exchanged materials showed lower apparent activation energy than the as-synthesized and calcined samples. It is interesting to note that the apparent activation energy was found to decrease with increasing the pore diameter in case of ion-exchanged samples. If internal diffusion was not limiting the catalyst, the apparent

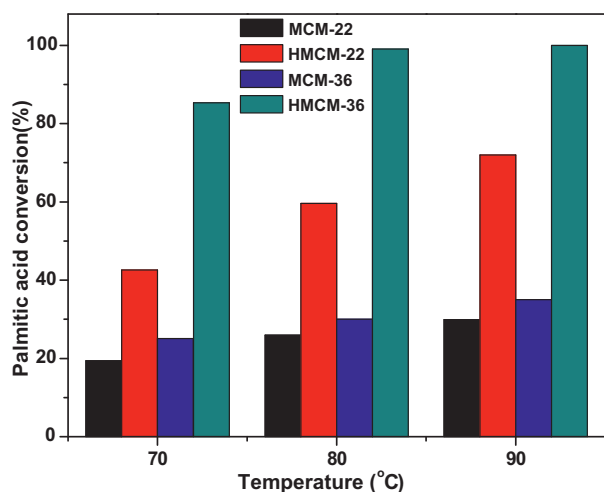


Fig. 8. Effect of reaction temperature on the conversion of palmitic acid over all the samples.

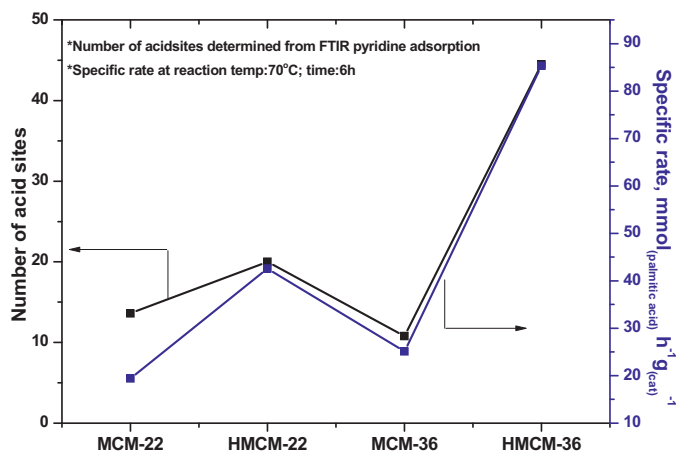


Fig. 9. Correlation between the number of acid sites and specific rate of all the catalysts.

activation energies for the synthesized MCM-22 and MCM-36 samples should be the same since these two samples possess only Lewis acid sites with small change in number of sites. A likely cause of the increase of apparent activation energy in these samples is due to less pore diameter which could hinder the diffusion of reactant molecules.

Mbaraka et al. [11] reported the importance of activated diffusion in the esterification of palmitic acid over the mesoporous catalysts. These authors also reported that materials should possess a pore size diameter at least within the range of 2–3 nm to avoid diffusion problems. The HMCM-36 sample possessed around 3 nm pore diameter as shown in Fig. 3(B). Fig. 9 presents the correlation between the total number of acid sites and specific rate for esterification of palmitic acid at 70 °C. It is clear that the specific rate of the esterification for catalyst proportional to the number of acid sites. In addition, HMCM-36 sample possesses higher Brønsted/Lewis acid ratio than other samples (Table 2). This observation coincides with the literature that esterification follows a Brønsted acid catalyzed pathway.

It is noted that HMCM-36 sample had significantly higher number of Brønsted acid sites than HMCM-22, and also the BET surface area of HMCM-36 was about twice as large as that of HMCM-22. It is known that the accessibility of the acidic sites, a potentially important characteristic is the strength of the acid site. Kirumakki et al.

Table 5  
Reuse of HMCM-36 in palmitic acid esterification.

Reaction time	Conversion of palmitic acid (%)			
	Cycle 1	Cycle 2	Cycle 3	Cycle 4
60	15.3	14.5	14.0	13.5
120	31.1	30.0	29.8	29.0
180	53.2	52.4	51.5	51.0
240	69.5	68.5	67.3	66.5
300	77.7	76.3	75.7	74.1
360	85.3	84.0	83.0	82.5

[31] reported that Si/Al ratio of zeolites (H $\beta$ , HY, and HZSM-5) influences the esterification with alcohols. It was also observed that the largest conversion values are obtained with low Si/Al ratios due to the Brønsted acid sites having been incorporated into the structure of MCM-41 [32].

Table 4 presents some results on esterification of palmitic acid over different mesoporous catalysts reported in the literature. It is clear that the pillared HMCM-36 in the esterification reaction offered high activity relatively at low reaction temperature. For the esterification of palmitic acid aimed at the production of biodiesel, HMCM-36 is active due to mesoporosity and large number of Brønsted acid sites. In order to study the catalytic stability of pillared HMCM-36 catalyst, an experiment, similar to the 'hot-filtration experiment' was carried out. The catalyst was suspended in the methanol for 24 h at reaction temperature 70 °C under stirring without addition of palmitic acid. After 24 h, the catalyst was separated from methanol by centrifugation, and the palmitic acid was added to the reaction mixture. The esterification reaction was carried out for 24 h, but the filtered methanol did not offer any activity. This observation indicating that the pillared HMCM-36 catalyst behavior is clearly heterogeneous in nature and there is no leaching of any active species. The dried catalyst was also tested for 6 h and the conversion of palmitic acid is same as the fresh catalyst. To evaluate the reusability of the most active catalyst, HMCM-36 the esterification of palmitic acid was repeated for four cycles (Table 5). After each cycle of the reaction, the catalyst was separated by filtration from the reaction mixture washed with methanol and dried at 70 °C. The dried catalyst was then reused for the next cycle. For each cycle, a fresh solution containing palmitic acid and methanol at the same concentrations as in the first cycle was prepared. A small decrease of activity was observed with each cycle, this result probably due to loss of amount of catalyst during the separation procedures.

#### 4. Conclusions

Porous MCM-22 and pillared MCM-36 has been synthesized by calcination and swelling/pillaring of MCM-22(P) material respectively. It was found that swelling and pillaring processes increased the BET surface area of MCM-36 by a factor of two and also the microporous nature of MCM-22 changed to MCM-36 with meso pores of around 3 nm. The ion exchanged MCM-22 and MCM-36 materials possessed more number of strong Brønsted acid sites. It was observed that HMCM-36 sample had the highest Brønsted/Lewis acid site ratio. The intrinsic activities of as-synthesized and ion exchanged materials were investigated by liquid phase esterification of palmitic acid with methanol to produce methylpalmitate. Based on the specific rates, HMCM-36 showed the highest reactivity. In addition, this reactivity was higher than that of the other mesoporous heterogeneous catalyst. Recycling esterification experiments suggested that the acid sites on HMCM-36 sample were stable and offered consistent activity for four cycles. The results of this study clearly indicating that HMCM-36 is a suitable catalyst for the production of methyl palmitate by the esterification

of palmitic acid due to its superiority in number of strong Brønsted acid sites and the mesoporous nature.

## Acknowledgements

This research work was funded by the Deanship of Scientific Research (DSR), King Abdulaziz University, Jeddah, under grant number (D-002-432). The authors acknowledge with thanks the DSR's financial support.

## References

- [1] J.A. Lercher, A. Jentys, In Handbook of Microporous Solids, in: F. Schuth, K. Sing, J. Weitkamp (Eds.), Wiley-VCH, Weinheim, Germany, 2002, pp. 1097–1145.
- [2] J.-O. Barth, A. Jentys, J. Kornatowski, J.A. Lercher, Chem. Mater. 16 (2004) 724–730.
- [3] J.Y. Ying, C.P. Mehnert, M.S. Wong, Angew. Chem. Int. Ed. 38 (1999) 56–77.
- [4] A. Jentys, K. Kleestorfer, H. Vinek, Micropor. Mesopor. Mater. 27 (1999) 321–326.
- [5] M. Mokhtar, K. Narasimharao, H.S. Harun, S.N. Basahel, I.H. Abd El-Maksod, Ceram. Int. 39 (2013) 683–689.
- [6] A. Clearfield, M. Kuchenmeister, Pillared Layered Materials, Supramolecular Architecture, ACS Symp. Ser. No. 499, in: T. Bein (Ed.), American Chemical Society, Washington, DC, 1992.
- [7] Y.J. He, G.S. Nivarthi, F. Eder, K. Seshan, J.A. Lercher, Micropor. Mesopor. Mater. 25 (1998) 207–224.
- [8] (a) A. Corma, V. Fornes, J. Martinez-Triguero, S.B. Pergher, J. Catal. 186 (1999) 57–63;  
(b) S. Maheshwari, E. Jordan, S. Kumar, F.S. Bates, R.L. Penn, D.F. Shantz, M. Tsapatsis, J. Am. Chem. Soc. 130 (2008) 1507–1516.
- [9] Y. Liu, E. Lotero, J.G. Goodwin Jr., J. Catal. 243 (2006) 221–228.
- [10] J.M. Marchetti, V.U. Miguel, A.F. Errazu, Fuel 86 (2007) 906–910.
- [11] I.K. Mbaraka, D.R. Radu, V.S.-Y. Lin, B.H. Shanks, J. Catal. 219 (2003) 329–336.
- [12] K. Narasimharao, A. Sridhar, A.F. Lee, S.J. Tavener, N.A. Young, K. Wilson, Green Chem. 8 (2006) 790–797.
- [13] J.M. Marchetti, A.F. Errazu, Biomass Bioenerg. 32 (2008) 892–895.
- [14] A.I. Tropecelo, M.H. Casimiro, I.M. Fonseca, A.M. Ramos, J. Vital, J.E. Castanheiro, Appl. Catal. A: Gen. 390 (2010) 183–189.
- [15] L. Xu, Y. Wang, X. Yang, X. Yu, Y. Guo, J.H. Clark, Green Chem. 10 (2008) 746–755.
- [16] M.E. Davis, Acc. Chem. Res. 26 (1992) 111–115.
- [17] W.J. Roth, J. Cejka, Catal. Sci. Technol. 1 (2011) 43–53.
- [18] S.-T. Yang, J.-Y. Kim, J. Kim, W.-S. Ahn, Fuel 97 (2012) 435–442.
- [19] W.J. Roth, J.C. Vartuli, C.T. Kresge, in: A. Sayari, et al. (Eds.), Nanoporous Materials II, Stud. Surf. Sci. Catal. 129 (2000) 501–506.
- [20] (a) M.E. Leonowicz, S.L. Lawton, R.D. Partridge, P. Chu, M.K. Rubin, Science 264 (1994) 1910–1913;  
(b) J. Cejka, A. Krejci, N. Zikova, J. Kotrla, S. Ernst, A. Weber, Micropor. Mesopor. Mater. 53 (2002) 121–133.
- [21] M. Lasperas, H. Cambo, D. Burnel, I. Rodriguez, P. Geneste, Micropor. Mater. 7 (1996) 61–72.
- [22] A. Corma, C. orell, J. Pérez-Pariente, Zeolites 15 (1995) 2–8.
- [23] J.A. Lercher, C. Grundling, G. Eder-Mirth, Catal. Today 27 (1996) 353–376.
- [24] J.-O. Barth, A. Jentys, J. Kornatowski, J.A. Lercher, Chem. Mater. 16 (2004) 724–730.
- [25] E.J.A. Schweitzer, P.F. van den Oosterkamp, Micropor. Mesopor. Mater. 20 (1998) 397–405.
- [26] B. de Rivas, C. Sampedro, M. Garcia-Real, R. Lopez-Fonseca, J.I. Gutierrez-Ortiz, Appl. Catal. B: Environ. 129 (2013) 225–238.
- [27] J.M. Jehng, A.M. Turek, I.E. Wachs, Appl. Catal. 83 (1992) 179–200.
- [28] F. Delannay, Characterization Of Heterogeneous Catalysts, Marcel Dekker, New York, 1984.
- [29] S. Unverricht, M. Hunger, S. Ernst, H.G. Karge, J. Weitkamp, Stud. Surf. Sci. Catal. 84 (1994) 37–44.
- [30] A. Palani, A. Pandurangan, J. Mol. Cat. A: Chem. 245 (2006) 101–105.
- [31] S.R. Kirumakki, N. Nagaraju, K.V.R. Chary, Appl. Catal. A: Gen. 299 (2006) 185–192.
- [32] B.R. Jermy, A. Pandurangan, Appl. Catal. A: Gen. 288 (2005) 25–33.
- [33] V.C. dos Santos, K. Wilson, A.F. Lee, S. Nakagaki, Appl. Catal. B: Environ. 162 (2015) 75–84.
- [34] A.C. Carmo Jr., L.K.C. de Souza, C.E.F. da Costa, E. Longo, J.R. Zamian, G.N. da Rocha Filho, Fuel 88 (2009) 461–468.
- [35] C. Poonjarernsilp, N. Sano, H. Tamon, Appl. Catal B: Environ. 147 (2014) 726–732.